UNLIMITED

BR78548

RAE TR 81005

LEVEL II

TR 81005

AD A107999

ROYAL AIRCRAFT ESTABLISHMENT

*

Technical Report 81005

January 1981

DTIC ELECTE NOV 24 1981 S D E

A THEORETICAL STUDY OF THE EFFECTS OF BODY SHAPE AND MACH NUMBER ON THE DRAG OF BODIES OF REVOLUTION IN SUBCRITICAL AXISYMMETRIC FLOW

by

D.F. Myring

*

DTIC FILE COPY

Procurement Executive, Ministry of Defence
Farnborough, Hants

UNLIMITED

81 10 27 534

UDC 533.696.5 : 533.6.013.12 : 533.6.011

ROYAL AIRCRAFT ESTABLISHMENT

Technical Report 81005

Received for printing 16 January 1981

A THEORETICAL STUDY OF THE EFFECTS OF BODY SHAPE AND MACH NUMBER ON THE DRAG OF BODIES OF REVOLUTION IN SUBCRITICAL AXISYMMETRIC FLOW

by

D. F. Myring

SUMMARY

Theoretical results of profile drag calculations for bodies of revolution at zero incidence in a uniform flow are presented for a range of body shapes and Mach numbers. At a fixed fineness ratio, nose and tail contours are shown to have little influence on the profile drag coefficient based on body volume to the power 2/3. Comparison with the ESDU data sheets shows good agreement. Results of a low drag study are shown to indicate that in terms of volume enclosed a body with a fineness ratio of about 5.5 is optimum and that a continuously changing radius distribution gives rise to a slightly lower drag than that of a body having a parallel-sided central section.

Departmental Reference: Aero 3496

Copyright
©
Controller HMSO London
1981

LIST OF CONTENTS

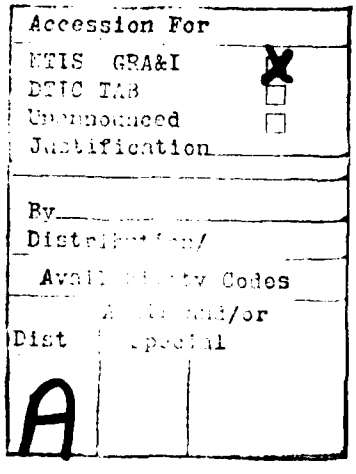

1 INTRODUCTION

Prediction of body drag is of interest in both the aeronautical and nautical fields. Examples such as fuselages, external store fairings and fuel drop-tanks come immediately to mind in aircraft applications whilst submarine and torpedo bodies are ready examples in the nautical world. The need for accurate prediction, though in some ways self-evident, is brought into sharper focus by the relative increases in size evident in modern subsonic fuselage design. Moreover, in many nautical applications body drag constitutes the major part of the resistance to motion under normal conditions, and thus plays a dominant role in determining range, maximum speed and so on.

The work presented here is intended as a contribution to the body of information[1] already available for the determination of body drag. It is in essence a refinement of existing data enabling the effects of detailed features of body design to be quantified and assessed. In practice body drag is affected by features such as wing and tail flow fields, body incidence and others. There is nevertheless a central part of the drag equivalent to the drag of an isolated body of revolution in axisymmetric flow, having the same area distribution as the real body. In many applications this part of the drag dominates drag increments due to incidence, camber, departures from symmetry and so on an is therefore worthy of study. Engineering Sciences Data Unit sheets dealing with this topic accommodate just one aspect of body geometry namely fineness ratio (length/maximum diameter). The results presented in this Report essentially confirm the trends evident from the data sheets[1] and go on to demonstrate the effects of detailed changes in nose and tail shapes. The theoretical basis of the calculation method is described in Ref 3. Any axisymmetric body shape may be specified, subject to the conditions of subcritical attached flow over the entire body surface. Boundary layer growth and surface pressure distribution are calculated iteratively assuming a viscous-inviscid interaction; the final matched solutions provide values of skin-friction and pressure drags. Comparison with Young's[2] predictions, which form the basis of the Data Sheets[1], will be shown to be very favourable. General agreement to within ±2% in total drag is evident even for fineness ratios as low as 5. A similar order of agreement with the Data Sheets is therefore implied.

Changes in profile drag with flow Mach number have been determined for different bodies and general trends are here illustrated for three different shapes. Total or profile drag is the sum of skin friction and pressure drags and for axisymmetric bodies at zero incidence in subsonic attached flows the pressure or form drag contributes only a few percent to the total drag. It might therefore be argued that as the flow Mach number rises the profile drag coefficient should fall, as does the skin friction coefficient. This is in fact the case, and the degree to which body shape affects the variation with Mach number is examined. Tail geometry and the detailed shape of the pressure distribution are shown to be significant factors. For some bodies pressure drag increases with Mach number but for others it falls. Design features which produce these trends are identified and it is shown that bodies with higher proportions of pressure drag tend to exhibit smaller reductions in profile drag coefficient as Mach number rises.

005

In many applications a reduction in profile drag brought about by careful design can be very beneficial. In the original work of Young[2] it was concluded that a fineness ratio of about 5 would afford an optimum volume carrying efficiency. More recently Hertel[4], from a study of the natural development of mammal and fish body shapes, has argued that in species renowned for their high speed motion fineness ratios of between 5.5 and 3.5 are typical. Thus if high speed swimming is associated with low drag then this coincides with Young's conclusion. Moreover, there would seem to be some evidence to suggest that a continuously changing radius distribution could offer some aerodynamic advantage over a parallel-sided body. These possibilities are investigated here in the form of a low drag study from which it is shown that the greatest savings come from the suppression of transition. Thus some care must be exercised in comparing flows typical of fish swimming at low Reynolds numbers with the flows at higher Reynolds numbers over bodies in aeronautical applications.

In order to make a parametric study of the effects of body shape on drag a family of bodies has been chosen which includes the modern cylindrical shape of the civil aircraft fuselage. However, the results are not intended to be exclusively centred on fuselage design although clearly this is a ready application. It is recognised that the profile drag of an isolated body is just one of several sources of drag which arise in practice which include examples such as wing-body interference, tail up-sweep and others. In particular it is emphasised that the low drag study is valid only for an isolated body.

2 THEORY

A full description of the theory used to predict drag has been presented in Ref 3, and here only a brief summary will be given in order to illustrate the salient features.

An iterative scheme is used to calculate an equilibrium condition between the viscous flow, confined to a boundary layer adjacent to the body and trailing downstream in a thin wake, and the outer potential flow which is assumed to be unbounded. An axisymmetric boundary layer method is used to calculate the displacement effect of the viscous region and the surface pressure distribution is determined by considering a fully inviscid flow over the body plus displacement effect. An iterative cycle is required because the displacement effect and the surface pressure distribution are mutually dependent.

Luxton and Young's[5] laminar boundary layer method is used up to a prescribed transition point downstream of which a compressible version of Head's[6] turbulent entrainment method is utilised. In the wake region further analysis is needed and the velocity profiles and entrainment rates are fully discussed. For the potential flow Hess and Smith's[7] formulations are adopted together with the Göthert transform[8] to allow for changes in density. At all times the flow is assumed to be subcritical and axisymmetric.

Undisturbed flow Mach number and unit Reynolds number must be specified as input parameters together with an assumed transition point. Different body shapes, defined in terms of a radius distribution, may be processed. Converged solutions contain surface pressure distributions and profile and form drags.

When compared with available experimental results the method shows good agreement in both surface pressures and drag. However, disparities are bound to appear at Mach numbers approaching the critical value for a given body, and in all the following calculated examples only Mach numbers well short of this are considered.

3 METHOD

It is possible, using the calculation scheme described in Ref 3, to examine theoretically the effects of detailed changes in body shape and free stream conditions. Many different families of body shapes may be invented, and the task of considering all of these is virtually impossible. Instead it is better to examine a single family which may include shapes not too far removed from current design trends, and to determine the benefits, if any, which may be derived from changes in detail or gross structure.

Modern fuselage designs consist almost universally of a cylindrical centre section of constant cross-sectional area, faired in by relatively short nose and tail sections. Fig 1a shows a model based on this observation. All dimensions are referred to the overall body length which is taken to be 100 units. A variable nose length, a, together with a mid-section of constant area and length b, fix the tail length as $(100 - a - b)$. Nose shape is based on a modified semi-ellipsoid and is given by the equation

$$r = \tfrac{1}{2}d\left\{1 - \left(\frac{x - a}{a}\right)^2\right\}^{\frac{1}{n}}, \qquad (1)$$

where r is the radius at axial station x and d is the maximum diameter. The nose index, n, may be varied to give different nose contours, a selection of which are depicted in Fig 1b for fixed values of a and d. With n equal to 2 the familiar semi-ellipsoid is obtained. Probably the most useful characteristic of different tail geometries is the tail semi-angle α, and Fig 1c shows the tail represented by a cubic curve in x for different values of α. A cubic curve is the simplest polynominal which may be determined by the requirements that the surface should pass through two given points with zero slope at one and a slope of $-\tan\alpha$ at the other, the trailing edge. Over the tail region the radius distribution is then given by

$$r = \tfrac{1}{2}d - \left\{\frac{3d}{2(100 - a - b)^2} - \frac{\tan\alpha}{(100 - a - b)}\right\}\{x - a - b\}^2$$

$$+ \left\{\frac{d}{(100 - a - b)^3} - \frac{\tan\alpha}{(100 - a - b)^2}\right\}\{x - a - b\}^3 . \qquad (2)$$

Thus, the complete body shape is a function of five independent parameters, namely a,b,n,α,d. In the following examples each body will be identified by a code in the form $a/b/n/\alpha/d$, where α is expressed in degrees.

Free stream conditions may be completely defined by two properties - Mach number and unit Reynolds number - which together with the axial transition station X_T complete

005

the problem specification. There are therefore no less than eight independent parameters to be considered.

Young[2] presented comprehensive results showing the effects of Reynolds number and transition point on drag, and calculations using the present method have substantially confirmed these predictions. Furthermore, compressibility in the subsonic regime and small detailed changes in body shape have not been found to alter the nature of the results significantly. In the major part of the results which follow, a constant value of Reynolds number of 10^7 based on body length is used and transition is fixed at 3% of the body length. These values are typical of wind tunnel model tests and this simplification considerably reduces the necessary calculation effort whilst detracting little from the final conclusions. A similar reduction in complexity with regard to the remaining parameters has also been observed. For the most part, the parameters have been found to be mutually independent in the sense that the effect of changing one parameter does not depend significantly on values of the remainder. Where slight dependencies are evident, they are quantitative rather than qualitative and do not affect the validity of the deductions.

Values of drag will be presented in coefficient form using $\frac{1}{2}\rho V^2 S$ as reference force. Here S is some characteristic area which must be specified for a given body. In the cases to be considered here, skin-friction forces constitute a major part of the resistance to motion and these depend strongly on surface area. A useful presentation may therefore be made using the total surface area, A, as reference. Coefficients defined in this way will be denoted by subscript A, so that the profile drag coefficient based on surface area will be written C_{DA}. Skin-friction drag coefficients will always be based on surface area and will be denoted C_{DF}.

It will be shown that drag coefficients based on surface area have the advantage that they are relatively insensitive to minor changes in surface area and may be used without detailed reference to body shape. However, when changes in profile drag are required as a result of contour changes a better representation is afforded by a coefficient based on some area which does not change with detailed shape. Here the surface area of a parallel sided cylinder of the same fineness ratio is used and coefficients based on this are denoted by subscript C. At a fixed fineness ratio, changes in C_{DC} produced by different nose and tail shapes give a direct indication of the changes in total drag force.

For some design problems a measure of volume carrying efficiency is required and here the obvious choice is a reference area equal to body volume to the power 2/3. Coefficients derived on this basis will be denoted by subscript V.

The following points should be noted as body diameter d tend to zero;

1. C_{DA} tends to equal C_{DF}.
2. C_{DC} tends to equal C_{DF}.
3. C_{DV} tends to infinity.
4. C_{DF} tends to the flat plate value.

Here C_{DA}, C_{DC} and C_{DV} all represent profile drag.

005

4 RESULTS

4.1 Incompressible flows - $M_\infty = 0$

Variations in C_{DC} with tail angle are shown in Fig 2, where fineness ratio is held constant. A range in angle from 0-26° is covered for two different bodies. It is worth noting that for all the shapes the calculated flow is far from separation over the entire body. The first body (15/55/1.25/-/10) is reminiscent of modern civil long range aircraft, although perhaps a little more slender. It has a short, relatively sharp nose and a tail 30 units long. A cusped tail evidently presents the least resistance to motion, with roughly an 8% rise in drag at $\alpha = 26°$. This rise is almost directly proportional to the increase in surface area of the blunter tail and owes very little to the change in surface pressure distribution.

A more pronounced effect is shown by the second body (25/25/1.25/-/10) which experiences a 16% rise in drag as the tail angle is increased from zero to 26°. Again this is a direct function of surface area which is here more sensitive to tail angle due to the longer tail (50 units). At a given tail angle the long-tailed body always has a smaller drag but the difference decreases as tail angle increases.

In this Figure, as in many others, the percentage change in drag covered by the graph is shown in the top left hand corner as an aid towards comparison between figures.

Changing the nose index, n, at constant tail angle ($\alpha = 10°$) leads to Fig 3 where again the second body with its long nose is more sensitive to changes in nose contour. As expected, bodies with blunt noses (large n) tend to have larger drags, and once more this is mostly due to larger surface areas. However, bodies with very blunt noses ($n > 3$) may produce localised regions of separated flow over the nose, which occur as a result of large adverse pressure gradients. When this happens further drag penalties are incurred and conditions outside the scope of the present method arise.

It is worth noting again that all configurations implied by Figs 2 and 3 have the same reference area since they have the same maximum diameter.

Drag coefficients based on surface area are shown in Fig 4 for the same two bodies, and here both curves exhibit definite minima in drag coefficient C_{DA}. For small increasing tail angles this means that the surface area is increasing at a greater rate than the local velocity peaks which were shown in Ref 3 to have a decisive effect on body drag. Beyond a certain angle the reverse is true and Fig 4 shows that the short-tailed body produces a minimum value of C_{DA} at a slightly larger tail angle. Again the long-tailed body is more sensitive to changes in tail angle, but it should be observed that Fig 4 covers only a 2% change in drag coefficient.

Young's[2] predicted value of C_{DA} for the same values of Reynolds number, fineness ratio and transition point is shown superimposed, and clearly this must be represented as being invariant with tail angle. It is nevertheless in good agreement with the mean of the two curves and even more so with the curve for the short-tailed body (15/55/1.25/-/10) at tail angles of about 16-20°. Overall a general agreement of ±1% with Young's value may be noted.

005

Variations in C_{DA} with different nose shapes are shown in Fig 5, in which the tail angle has a constant value of 10^{o}. Here a smaller change in drag coefficient is exhibited (about 1.5%) but it may be deduced that C_{DA} falls slightly as the nose becomes blunter but rises as it becomes shorter. Young's value of C_{DA} is in very good agreement with the curve for the short-tailed body and this is due to the similarlity between this body and the one considered by Young. An agreement to within 1% may be observed in Fig 5 and it is evident that short blunt noses tend to have the same values of C_{DA} as long sharp ones.

A steadily rising value of C_{DV} (based on volume$^{2/3}$) follows from increasing the value of the tail angle α. This is shown in Fig 6 where again the long-tailed body is seen to produce lower values of drag coefficient. The differences produced by the two bodies are small for tail angles in the region of 12^{o} and over the range $0\text{-}26^{o}$ in α, C_{DV} changes by only 1% for each body. It may be concluded that the drag force rises only marginally faster than volume to the power 2/3 and for a given volume is smallest for long cusped tails. A value of C_{DV} may be extracted from Young's analysis by assuming a standard shape of the R101 airship and then relating surface area to volume. For a fineness ratio of 10 this gives the relation

$$\text{Volume}^{2/3} = 0.126\ (\text{surface area}) \qquad (3)$$

which leads to a value of C_{DV} of 0.025107 for the conditions of Fig 6. Again this is shown to be within ±1% of the curves for both bodies over the full range of tail angles.

Nose shape affects C_{DV} even less than it affects C_{DA}. This may be seen in Fig 7 where at $\alpha = 10^{o}$ changing the nose index n has very little effect. In fact, for the short-tailed body (15/55/-/10/10) a shallow maximum in C_{DV} occurs at $n = 2$ (elliptic nose) with both blunter and sharper noses giving smaller values. The other body (25/25/-/10/10) shows a tendency towards a maximum value of C_{DV} at a larger value of n, but this is outside the range of the present graph. Less than ½% variation in C_{DV} may be observed over the complete range of nose shapes considered and agreement with Young's predicted value is again very good.

Form drag may be obtained by subtracting skin-friction drag from profile drag, so that

$$\frac{\text{form drag}}{\text{profile drag}} = 1 - \frac{\text{skin friction drag}}{\text{profile drag}} = 1 - \frac{C_{DF}}{C_{DA}}. \qquad (4)$$

Fig 8 may therefore be interpreted as a representation of percentage form drag variations, although in fact the ratio $\frac{C_{DF}}{C_{DA}}$ is plotted against tail angle. The same two bodies are considered (15/55/1.25/-/10, 25/25/1.25/-/10) and it can be seen that the long-tailed body has a smaller percentage form drag which has a minimum value of about 3% at $\alpha = 12^{o}$. At larger tail angles the form drag rises to 4% of the profile drag. The short-tailed body has a minimum percentage form drag of about 4½% at $\alpha = 17^{o}$ and this changes very

005

little over the full range of tail angles. As expected, Young's predicted percentage form drag is in good agreement with that of the latter body which on average is about 1% greater than that of the former body.

In Fig 9 skin-friction drag coefficients are plotted against tail angle α, and here again minimum values occur at roughly the same values of α as for the profile drag minima. Generally the skin-friction drag coefficients are larger than that predicted by Young, particularly in the case of the long-tailed body, which is more sensitive to tail angle. Total variations over the range of tail shapes amount to approximately 2%.

Similar curves are shown in Figs 10 and 11 but here changes in nose shape are considered. From Fig 10 it may be concluded that long thin noses produce smaller values of percentage form drag when compared with short blunt ones which show definite increases. The position is somewhat reversed in Fig 11 where clearly blunt noses produce lower skin-friction drag coefficients and this reduction tends to be enhanced by shortening the nose length. However, changes in nose length affect C_{DF} to a small degree when compared with changes produced in the percentage form drag. Agreement with Young[2] is within 1% for both figures.

So far results for a single fineness ratio of 10 have been presented, and at different fineness ratios very similar trends have been calculated. For fineness ratios as low as 5 agreement with Young remains well within ±2% for profile drag coefficients. The effects so far discussed may therefore be summarised by the observation that long sharp noses and tails have a beneficial effect on drag in incompressible flows. This is mainly due to a reduction in surface area and also a tendency to reduce the velocity peaks in the potential flow. At the same time, volume-carrying efficiency is increased, as shown by decreasing values of C_{DV} in Figs 6 and 7. However, the increase in efficiency is only of the order of 1% over the present range of shapes. Long noses and tails tend to have larger skin-friction drag coefficients which are decreased by increasing the nose and tail bluntness. Form drag as a percentage of profile drag is increased by short blunt noses and has a minimum value at a certain tail angle which depends on tail length. As tail length increases percentage form drag falls.

Changes in drag with thickness ratio (the reciprocal of fineness ratio) are shown in Figs 12 and 13 in terms of the three coefficients C_{DA}, C_{DC} and C_{DV}. In these figures the length and shape of both the nose and tail have been kept constant and the maximum thickness varied. Variations of up to 12% are evident in Fig 12 as the body thickness is doubled. Increases in C_{DA} with thickness ratio as predicted by Young are seen to be in excellent agreement with the present calculations. Increases in C_{DC} shown in Fig 13 are smaller (about 9% as body thickness is doubled) but this is simply due to larger changes in reference area. Really significant trends are exhibited by the curve of C_{DV} against thickness ratio which shows a shallow minimum at a value of d/L of approximately 0.20. Roughly 8% increase in volume carrying efficiency is produced by halving the fineness ratio and this is due to a more efficient use of surface area to contain a given volume. Young predicted a very similar result when he considered the most desirable thickness ratio to carry a given volume. He also obtained a value of 0.20

005

although in his case the body Reynolds number varied slightly because thicker bodies have a smaller length for a fixed volume. However, the shallow minimum in Fig 13 and the small sensitivity to Reynolds number have led to the same result here. Calculations have been made for several different nose and tail contours, but the optimum value of thickness ratio was not found to vary significantly. In fact it showed a slight tendency to rise for long sharp noses and tails.

Fig 14 shows calculated external velocity distributions for three different bodies and provides a representative picture of the effects of contour changes. The two nose and tail length combinations considered in Figs 2 to 11 are labelled B and C and their profiles are shown. Body C is the long-tailed body and here has a cusped tail and a nose index of 1.25. Body B has a shorter nose with the same index but has a tail angle of 25°. The effect of nose lengthening is to reduce the peak velocity over the nose and at the same time to displace its position in a downstream direction. This rearward movement of the velocity peak may lead to some rearward movement of the transition point in a real flow, whilst the reduction in peak velocity tends to reduce the drag. In the tail region velocity perturbations are reduced by increasing the tail length and decreasing the tail angle. An upstream movement of the tail peak velocity is also discernible. The net result is a reduction of the adverse pressure gradients where the boundary layer is thickest and again this tends to reduce the drag. Pressure at the tip of the tail region is dramatically reduced by the long, cusped tail. Over the parallel sided midsection the long-tailed body has a higher velocity which tends to produce larger shear forces, but overall it shows a 1.65% reduction in C_{DV} over the short-tailed body. It is therefore a more efficient shape when used to carry a given volume.

Body A of Fig 14 shows how increases in body thickness affect the velocity distribution. It has a nose index of 1.50, a tail angle of 10°, and nose and tail lengths identical to those of body B. The increased thickness leads to larger perturbation velocities and roughly doubles the peak perturbations of body B. Over the nose the peak velocity occurs in almost identical positions for bodies A and B, but the smaller tail angle of body A pushes its tail peak upstream compared with that of body B. This also leads indirectly to a lower tail tip pressure for body A. A 7.5% reduction in C_{DV} is shown by body A when compared with body B and this again indicates that increasing thickness is a much more effective way of increasing the volume carrying efficiency when compared with the smaller increases obtained by changes of body contour at a fixed thickness.

4.2 Compressible flows

Trends shown by the results already presented are not significantly affected by changes in free-stream Mach number, but body geometry has an observable effect on the variations of profile and form drag with Mach number. To illustrate this point bodies B and C of Fig 14 have been considered at a series of Mach numbers up to $M_{\infty} = 0.8$, which is well short of the critical value. It is convenient to present the results in the form C_D/C_{Di}, where subscript i represents the equivalent drag coefficient in incompressible flow but otherwise identical free-stream conditions. Thus Fig 15 shows C_{DA}/C_{DAi} and C_{DF}/C_{DFi} plotted against Mach number for bodies B and C. Also shown is the variation of

005

flat plate drag with Mach number, which may be obtained from the skin-friction law used in Ref 3 as

$$\left[C_{DF}/C_{DFi}\right]_{\text{flat plate}} = (1 + 0.1295\ M^2)^{-0.6}\ , \qquad (5)$$

in which transition has been assumed to occur at the leading edge. Reference to Fig 15 shows that the skin-friction drag of body B falls less rapidly with increasing values of Mach number than does the flat-plate drag. Body C shows a slightly increased tendency towards lower skin-friction drag as the Mach number rises, with almost identical variations in both profile and skin-friction drag. On the other hand the profile drag of body B falls less rapidly than the skin-friction drag. This difference in behaviour between the two bodies is strongly associated with the larger percentage form drag of body B. Fig 16 shows that at $M_\infty = 0$ body B has a greater percentage form drag and the increase in this percentage with increases in Mach number is more marked than that of body C which is hardly affected. This accounts for the differences in separation in the profile drag and skin-friction drag curves in the previous figure.

To summarise the effects of compressibility it may be said that increasing values of Mach number decrease the drag coefficient of a flat-plate, all other conditions being kept constant. For bodies of finite volume in subcritical flows the skin-friction drag coefficient falls to a lesser extent and this is due to increased velocity perturbations in the potential flow, resulting from density changes; the bigger the velocity perturbations in incompressible flow the smaller the decrease in C_{DF} with rising values of Mach number.

Profile drag coefficients decrease with increasing Mach number but to a lesser extent than C_{DF} . Decreases in C_{DA} tend to be smaller for bodies with larger proportions of form drag.

It should be noted that the effects of compressibility so far discussed are independent of the coefficient reference area since reference to incompressible conditions has been made throughout.

4.3 Low drag study

Having determined the effects of various changes in body shape the first stages of a low drag design may now be discussed. First, a design aim must be set. Several possibilities may be imagined, and of these a low drag study at a fixed volume has been chosen. The aim is therefore to design a body with a low drag to transport a given volume at a certain Reynolds number and Mach number. The following considerations are of prime importance;

(1) C_{DV} should be as low as possible, although some small sacrifices may be made on grounds of structural practicalities.

(2) The surface pressure distribution should not show large negative peaks as these would lower the critical Mach number, above which significant wave drag may appear.

500

(3) Although a fixed transition station at $d/L = 0.03$ will be assumed, the first minimum pressure point (or peak velocity) should be as far downstream as possible since it is known[9] that this tends to delay the onset of transition in real flows.

Each design feature may be discussed in turn assuming small interdependence.

(a) Thickness ratio

Fig 13 shows that this is a powerful parameter for changing C_{DV} and a value near the minimum point is required. However, having noted that increased thickness leads to increased velocity peaks (Fig 14) a value of d/L of 0.18 is judged to be more suitable than 0.20. The difference in C_{DV} is very small whilst at the same time a higher critical Mach number is obtained.

(b) Nose shape

Long slender noses have a tendency to push back the first velocity peak (Fig 14) and also tend to decrease C_{DV} (Fig 7). However, if the maximum section occurs too far downstream large adverse pressure gradients may arise over the tail region where the boundary layer is thickest. A nose 50 units long, with an index of 2 has been found to produce the best compromise. A lower nose index gives bodies with rather sharp noses which are structurally and practically undesirable, whilst a higher index tends to increase the peak velocity and move its position upstream. Fig 7 shows that nose index has only a very small influence on C_{DV}.

(c) Tail shape

Again, long slender shapes tend to give low values of C_{DV}. By removing the parallel sided mid-section of the body the second velocity peak may also be removed, and this produces smaller adverse gradients over the tail. A tail 50 units long is therefore desirable. Small tail angles of below about 8° are impractical, and for the long-tailed body Fig 6 shows only a 0.4% increase in C_{DV} as α changes from $8\text{-}25^{\circ}$. This figure tends to rise with body thickness, but for a d/L of 0.18 it remains well short of 1%. A 25° tail may therefore be used to considerable constructional advantage with very little penalty in drag coefficient. In this particular configuration a blunt tail tends to lower the peak velocity in the tail region, which is also an advantage.

Within the family of shapes considered a low drag shape of 50/0/2/25/18 has therefore been deduced, and this is a shape with continuously varying cross-sectional area, an ellipsoid nose, a tail of equal length with a 50° included angle, and a fineness ratio of 5.556.

Calculated values of drag coefficient C_{DV} are shown in Fig 18 for a range of Mach numbers up to $M_{\infty} = 0.8$. Curves for bodies B and C (shown in Fig 14) are compared with the low drag body results which are about 10% lower in value. Of this 10%, 8% is due to increased thickness ratio and 2% to changes in nose and tail contours, as may be seen in Fig 13. Rising values of Mach number tend to have less effect on C_{DV} for the low drag body and this reduces the differences in drag by about 1% at $M_{\infty} = 0.8$. As noted previously bodies with higher proportions of form drag invariably exhibit a smaller

005

tendency towards lower drag coefficients in compressible flows. Young[2] predicted form drag percentages to be given by

$$\frac{\text{form drag}}{\text{profile drag}} \simeq 0.4\,\frac{d}{L}\,, \tag{6}$$

for imcompressible flows and this is depicted in Fig 17 in the form C_{DF}/C_{DA} versus d/L . Also included are results obtained by increasing the thickness of a (15/55/1.5/10/-) body which give values of form drag higher than those of Young. However, the single point for the low drag body is close to Young's curve, and this is because it is similar in shape to the thick body treated by Young[2]. Fig 17 clearly shows that percentage form drag depends to a much greater extent on nose and tail shapes than does profile drag. The percentage form drag of the low drag body is roughly twice that of body C, and hence the differences in sensitivity to flow Mach number shown in Fig 15 are to be expected. Nevertheless, the aim of reducing C_{DV} has been achieved and the improvement in drag becomes only slightly less as the Mach number rises.

Calculated external velocity distributions may be seen in Fig 19, where, compared with body B, the peak velocity of the low drag body is well downstream and at a somewhat lower level. Also, the second peak does not occur, and as a result the tail pressure gradients are slightly smaller than those of body B. Tail tip pressures are virtually identical in the two cases and overall the low drag body has a velocity distribution with the required characteristics of a small velocity peak resident at a station well downstream of the nose.

To put the drag reduction in true perspective Fig 20 must be considered. Here the low drag body is compared with a body of equal volume having a fineness ratio of 10. The latter is in fact body B as discussed previously, and in order to contain the same volume it must be 36.1% longer than the low drag body. It will be seen that the forward nose shapes are not dissimilar, and the tail angles are identical. For the same flight conditions and with transition fixed at $x/L = 0.03$ the increased body Reynolds number of the slender body reduces the drag advantage of the low drag body to 7.26%. At very low Reynolds number the transition points will tend to occur at the peak velocity station and in this case a drag advantage of over 60% will be afforded by the low drag body.

5 DISCUSSION

In many ways it is helpful to consider the individual contributions of skin-friction and pressure forces to total drag. This leads to a better understanding of the effects and limitations of design features and free stream flow conditions.

By far the greater part of the resistance to motion comes from skin-friction forces which are greater than 90% of the total resistance for all bodies considered here. This is mostly due to the avoidance of separated flows which may lead to large pressure drags. The main factors which determine skin-friction drag may be observed in the following relationship;

$$\text{skin-friction drag} \;\propto\; \int_0^L \rho u^2 c_f \, dx\,. \tag{7}$$

005

Flat-plate drag may be obtained by putting r equal to plate width (normal to stream). Now consider the skin-friction drags of a flat-plate and a body of equal wetted area and similar transition points. Figs 14 and 19 show that finite body volume leads to values of ρu^2 in excess of the undisturbed value local to the flat plate, and from the above equation a tendency towards increased skin-friction drag may be predicted. At the same time, values of c_f will differ between the body and plate, but the overwhelming effect is the change in local dynamic head. Hence the skin-friction drag of the body will exceed that of the plate simply because of the positive velocity perturbations produced by its bulk.

In high-speed flows changes in density result from velocity perturbations such that the velocity changes tend to be amplified. This is shown in Fig 19. The net effect is an amplification of changes in dynamic head. Local values of Mach number in excess of the flat-plate value lead to smaller values of c_f (more particularly in turbulent rather than laminar boundary layers), but again the increased values of ρu^2 are dominant. Thus with increasing values of Mach number, flat-plate drag falls more rapidly than body drag due to skin friction. Fig 15 shows that the skin-friction drag of the low drag body is least reduced by increasing Mach number. This is because, although it has a smaller peak velocity than body B, Fig 19 indicates that the velocity perturbations occur over a greater surface area and hence affect the total surface shear stress to a greater extent. On the other hand, body C has smaller velocity perturbations over a smaller area and has the greatest reduction in skin-friction drag as Mach number rises.

Changes in body geometry affect skin-friction drag in two ways. First, the velocity distribution is changed and secondly the surface area presented to the flow is altered. If the velocity peaks shown in Figs 14 and 19 could be induced to reside over regions of small radius, a reduction in skin-friction drag would be obtained. Unfortunately, this is not an easy procedure since making the nose or tail more slender simply pushes the velocity peaks onto the thick regions of the body. Hence the sensitivity to nose shape is very small, but as can be seen from Fig 11 short blunt noses tend to give lower skin-friction drag coefficients. Tail shapes have very similar effects. Increasing body thickness has a tendency to present a greater surface area to locally increased velocities and as a result the skin-friction drag coefficient rises.

In subsonic flow, form drag is due entirely to the displacement effect of the boundary layer; in particular to the absence of a rear stagnation point which would be present in inviscid flow. For bodies with long parallel-sided centre sections, negligible form drag is produced by nose pressures; hence the small sensitivity to nose shape in Fig 10, where long sharp noses have only a small tendency towards a reduction in form drag. A more significant effect is seen in Fig 17 where increases in thickness ratio increase the percentage form drag. As might be expected, the more slender nose and tail of the low-drag body lead to decreases in form drag when compared with the 15/55/1.5/10/- body at the same thickness ratio.

Compressibility effects on form drag are more difficult to assess. Fig 21 shows form drag referred to incompressible values for three bodies. The low drag body, which

005

has the highest form drag, shows a 5% increase in form drag at $M_\infty = 0.8$ and body C, with the lowest form drag, shows a 2% decrease. Body B, with an intermediate value of form drag, shows a much larger 13% increase at $M_\infty = 0.8$. Body B, because of its geometry, has very little nose pressure drag, so that, referred to undisturbed ambient pressure, it must experience a tail suction force. As M_∞ rises all pressure perturbations increase including the tail suction pressures. The low drag body experiences a nose suction force opposing the larger tail suction force. As M_∞ increases a smaller increase in form drag is therefore felt. In the case of body C, with a cusped tail, nose suction forces initially increase more rapidly than tail forces and so the form drag falls with increasing Mach number. As a general rule it may be said that bodies with nose pressure distributions almost independent of tail shape suffer increases in form drag with rising Mach number. For bodies with shorter centre-sections the increase is not so marked, especially at small tail angles. As tail angle decreases and length increases pressure drag eventually begins to fall with increasing Mach number. This explains the differences in compressibility effects shown in Fig 15.

In many applications the most relevant profile drag coefficient is that based on volume to the power 2/3, since this allows a direct comparison of volume carrying efficiency. Figs 6 and 7 show that long sharp noses and tails tend to give lower values of C_{DV} , whilst from Fig 13 an optimum value of thickness ratio may be deduced at which C_{DV} has a minimum value. All of these phenomena may be explained by the observation that for a given volume a spherical shape has the least surface area. By making the nose and tail more slender and at the same time increasing the body thickness ratio, a shape more like that of a sphere is produced. Skin-friction drag, which is closely related to surface area, is therefore decreased if the volume is kept constant. However, form drag increases with thickness ratio and tends to offset the lower skin-friction forces. An optimum condition is reached when increments in skin friction and pressure drags are equal and opposite.

For a given body the effect of increasing the flow Mach number is to decrease the profile drag coefficient. Although the detailed variation depends on body shape, as a general rule bodies with higher proportions of form drag tend to show smaller decreases. Hence, thin bodies with long sharp noses will be subject to relatively larger variations in drag coefficient with Mach number than will thick bodies with short blunt noses. This may be seen in Fig 15. It is of interest to note that measurements and calculations performed for two-dimensional wing sections[10] have shown little change in drag coefficient with increases in Mach number below the critical value, and again this may be associated with higher proportions of form drag which are roughly twice those of axisymmetric bodies having the same thickness ratios.

The low drag body design is somewhere near an optimum practical shape for an isolated body. Sharp ends have been avoided and the final area distribution is continuously changing with axial position. A low value of C_{DV} is mainly due to the adoption of a thickness ratio near the optimum value, changes in nose and tail contours being much less effective in this respect. However, nose and tail shape have been varied to produce

005

a desirable pressure field which determines the critical Mach number and may have a strong effect on the position at which transition occurs. At a given volume and transition point, a saving of about 7% in drag has been obtained relative to more typical fuselage designs, with no decrease in critical Mach number. If transition is assumed to occur at the first peak velocity point then the saving in drag increases to about 60%. Hence, it must be concluded that Hertel's observations of body shapes were mainly concerned with the location of transition to turbulent flow rather than the most effective use of surface area. In the case of fish, which swim at low Reynolds numbers, the point of transition is largely governed by pressure gradients, whereas at the high Reynolds numbers of aircraft fuselages transition will in all events occur near the nose.

Overall agreement with Young's calculated values of profile drag coefficient has been found to be within ±1% for a fineness ratio of 10 and a transition station at $x/L = 0.03$. A wide range of body shapes has been examined, but due to the direct relationship between surface area and drag the coefficient C_{DA} changes only slightly with variations in nose and tail contour. A typical variation over a range of Reynolds numbers is shown in Fig 22 where it will be seen that Young's results lie slightly above the present calculations. For thicker bodies the drag coefficient C_{DV} is less dependent on nose and tail shapes than C_{DA} . This may be seen in Figs 12 and 13 where for the low drag body C_{DV} differs by only 1.8% relative to the other family of bodies, whereas C_{DA} differs by 4%. Hence, if coefficients of profile drag are based on volume to the power 2/3 then agreement to within ±2% between bodies of very different shapes is obtained. Values of form drag percentage depend rather more on the detailed shape of the surface pressure distribution, and it will be seen from Fig 17 that agreement with Young's values is good only when similar bodies are considered. Fig 23 shows how Reynolds number affects the percentage form drag. At higher Reynolds numbers the boundary layer displacement thickness is smaller and the form drag less. The corresponding changes in pressure distribution are shown in Fig 24 at two Reynolds numbers. Better tail pressure recovery at the higher Reynolds number is clearly evident.

6 CONCLUSIONS

(1) Fineness ratio is found to have the dominant effect on profile drag for axisymmetric bodies of fixed volume. Detailed design of the nose and tail also influences the profile drag but to a much lower degree.

(2) A low-drag body has been designed which has a fineness ratio of 5.5 and a drag 7% less than that of a body shaped like a conventional aircraft fuselage (fineness ratio 10). On this low-drag body, as with all the calculations made, the boundary layer is attached throughout and is well away from separation conditions.

(3) At a given fineness ratio, Reynolds number and transition point, profile drag coefficients based on volume to the power 2/3, C_{DV} , are less dependent on body shape than coefficients based on surface area, C_{DA} . For fineness ratios of order 10 agreement with Young's results to within ±1% is obtained in terms of C_{DA} and C_{DV} . At a fineness ratio of 5 the agreement falls to ±4% in C_{DA} and ±2% in C_{DV} . These results hold for a wide range of Reynolds numbers and transition points.

005

(4) Form drag depends to a greater extent than skin-friction drag on detailed body shape, and for bodies similar to Young's almost identical values of form drag have been calculated. Increasing values of Reynolds number lead to lower form drag percentages and higher tail tip pressures.

(5) Increases in Mach number produce decreases in profile drag coefficient to a degree which falls as percentage form drag rises. Hence, little change in profile drag coefficient with Mach number is observed for bodies with high proportions of form drag.

(6) A continuously varying cross-sectional area distribution leads to smaller peak velocities occurring at stations further downstream and as a result higher critical Mach numbers may be obtained.

005

List of symbols

A	body surface area
a	nose length
b	length of parallel sided mid-section of body
C_{DA}	profile drag coefficient based on surface area A
C_{DV}	profile drag coefficient based on volume$^{2/3}$
C_{DC}	profile drag coefficient based on surface area of cylinder
C_{DF}	skin-friction drag coefficient based on area A
c_f	skin-friction coefficient
d	maximum body diameter
L	body length
M	Mach number
n	nose index
R_L	Reynolds number based on body length
r	body radius
S	general reference area
u	resultant velocity
V	free stream velocity
x	axial distance measured from body nose
x_T	transition station
α	tail semi-angle

subscripts

i	incompressible conditions
∞	conditions at infinity

REFERENCES

No.	Author	Title, etc
1	-	ESDU Data Sheets.
2	A.D. Young	The calculation of the total and skin-friction drags of bodies of revolution at zero incidence. R & M 1874 (1939)
3	D.F. Myring	The profile drag of bodies of revolution in subsonic axisymmetric flow. RAE Technical Report 72234 (1973)
4	H. Hertel	Structure form and movement. Reinhold Publishing Corporation
5	R.E. Luxton A.D. Young	Generalised methods for the calculation of the laminar compressible boundary layer characteristics with heat transfer and non-uniform pressure distribution. R & M 3233 (1962)
6	M.R. Head	Entrainment in the turbulent boundary layer. R & M 3152 (1960)
7	J.L. Hess A.M.O. Smith	Calculation of potential flow about arbitrary bodies. Prog. Aero. Sci. Vol.8 (1967)
8	B. Göthert	Jahrb. d. Deutsch. Luftfahrtforschung (1941)
9	H. Schlichting	Boundary layer theory. Sixth Edition - McGraw-Hill (1968)
10	J.F. Nash J. Osborne A.G.J. Macdonald	A note on the prediction of aerofoil profile drag at subsonic speeds. NPL Aero Report 1196 (1966)

REPORTS QUOTED ARE NOT NECESSARILY AVAILABLE TO MEMBERS OF THE PUBLIC OR TO COMMERCIAL ORGANISATIONS

500

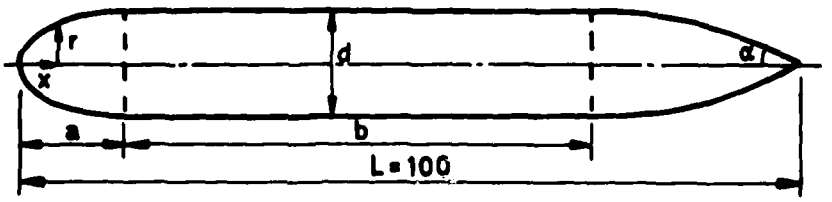

a Overall shape

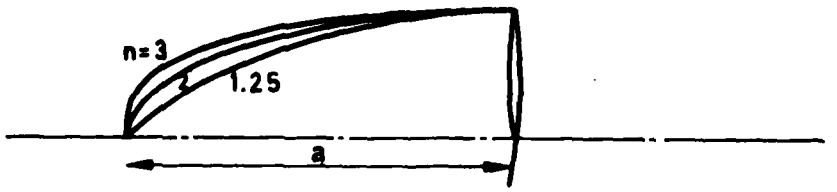

b Nose shapes

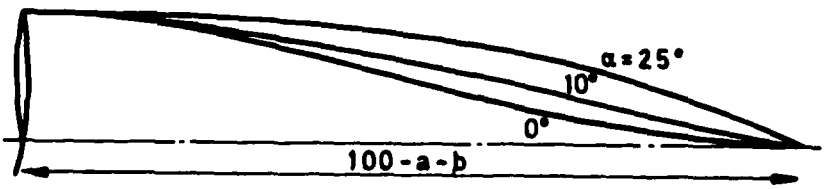

c Tail shapes

Fig 1a-c Body geometry

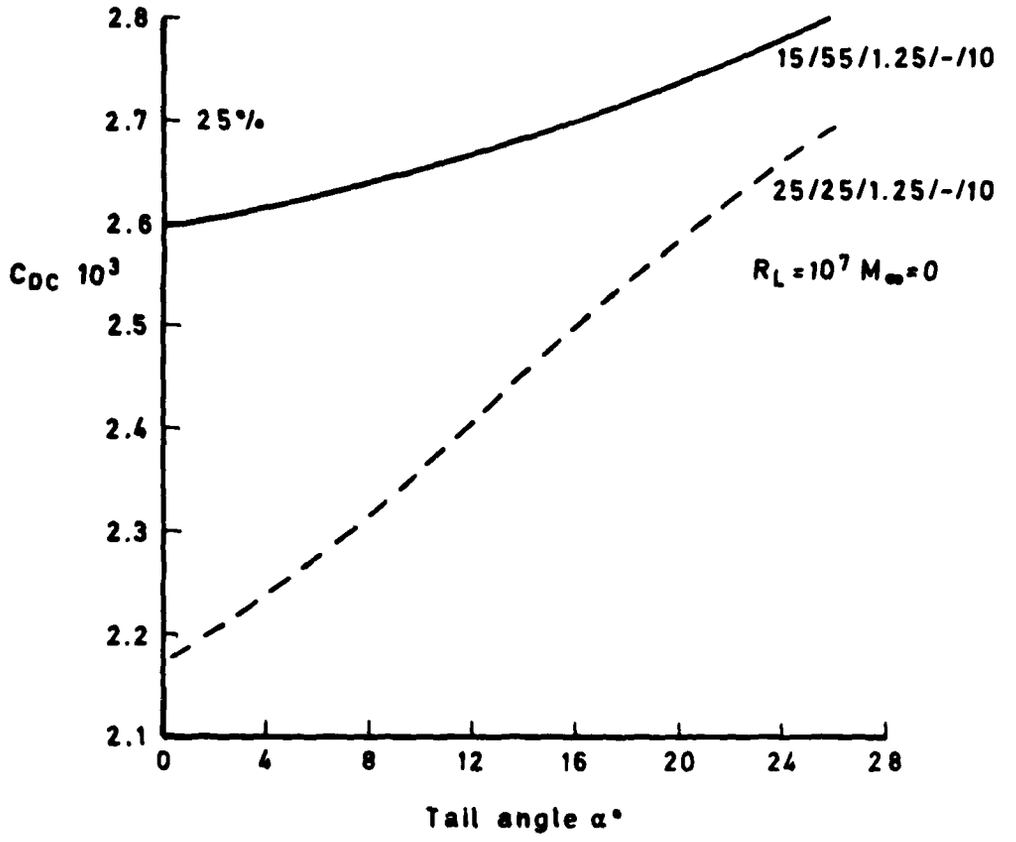

Fig 2 Effect of tail angle on drag coefficient based on cylinder

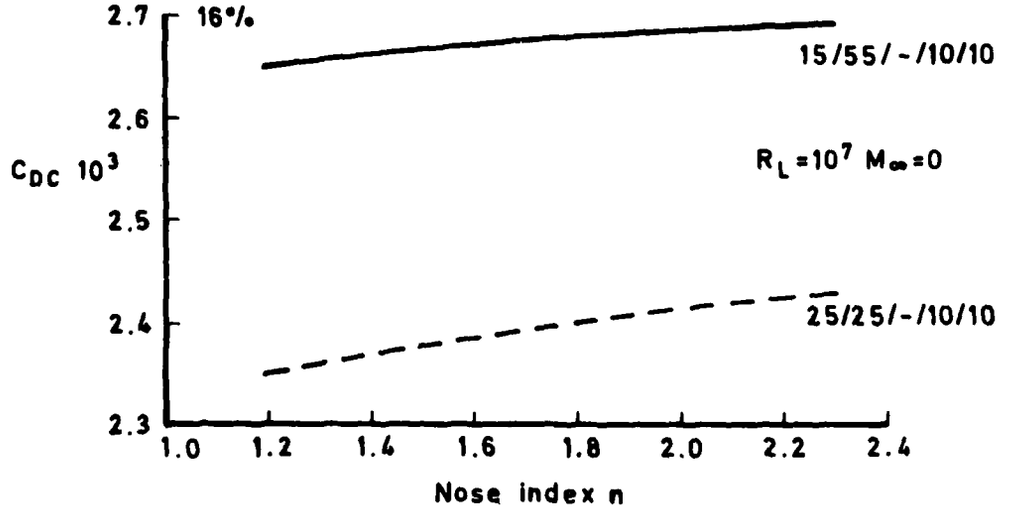

Fig 3 Effect of nose shape on drag coefficient based on cylinder

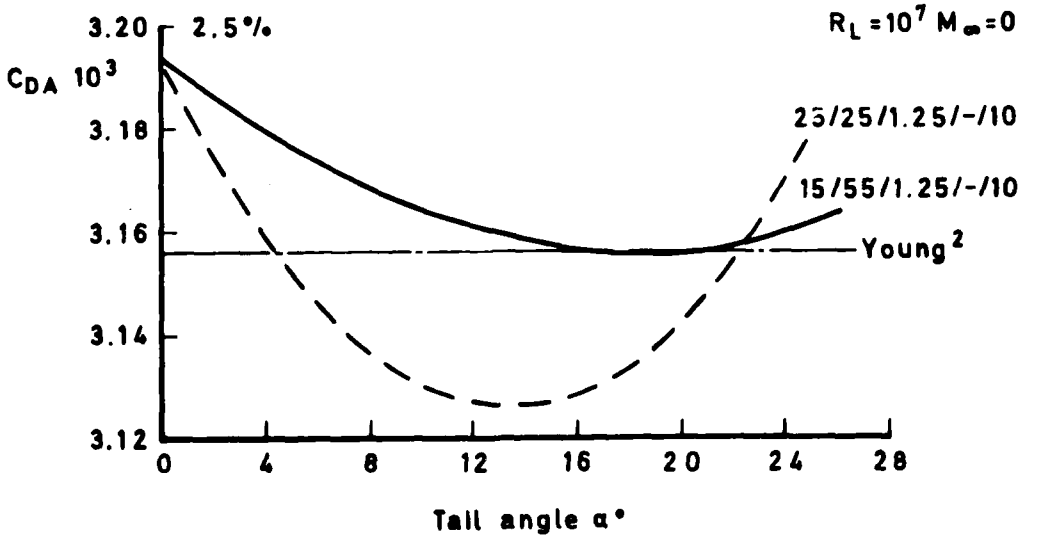

Fig 4 Effect of tail angle on drag coefficient based on surface area

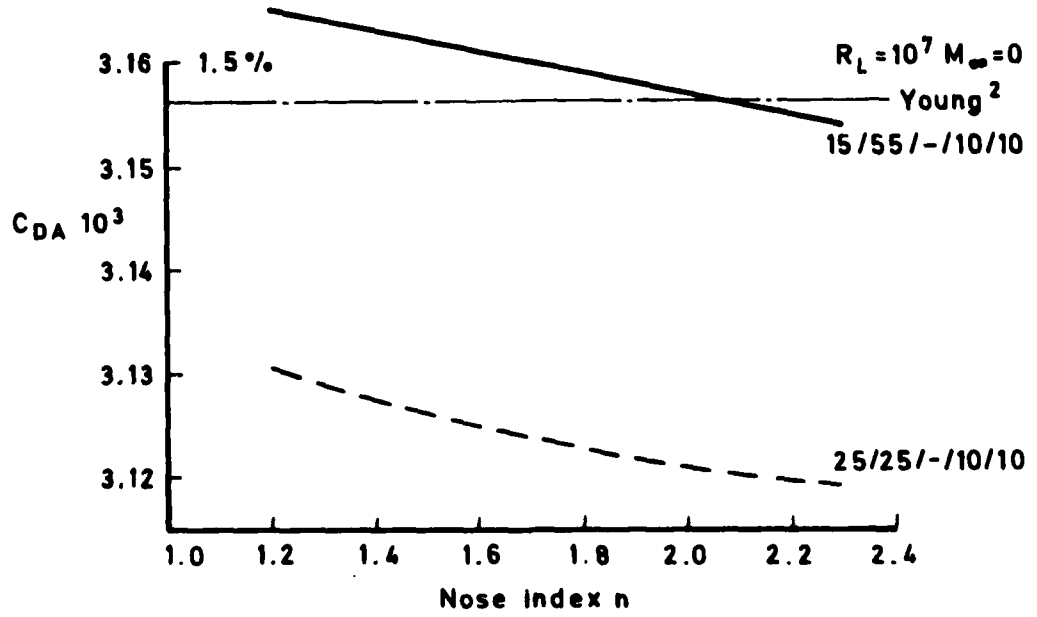

Fig 5 Effect of nose shape on drag coefficient based on surface area

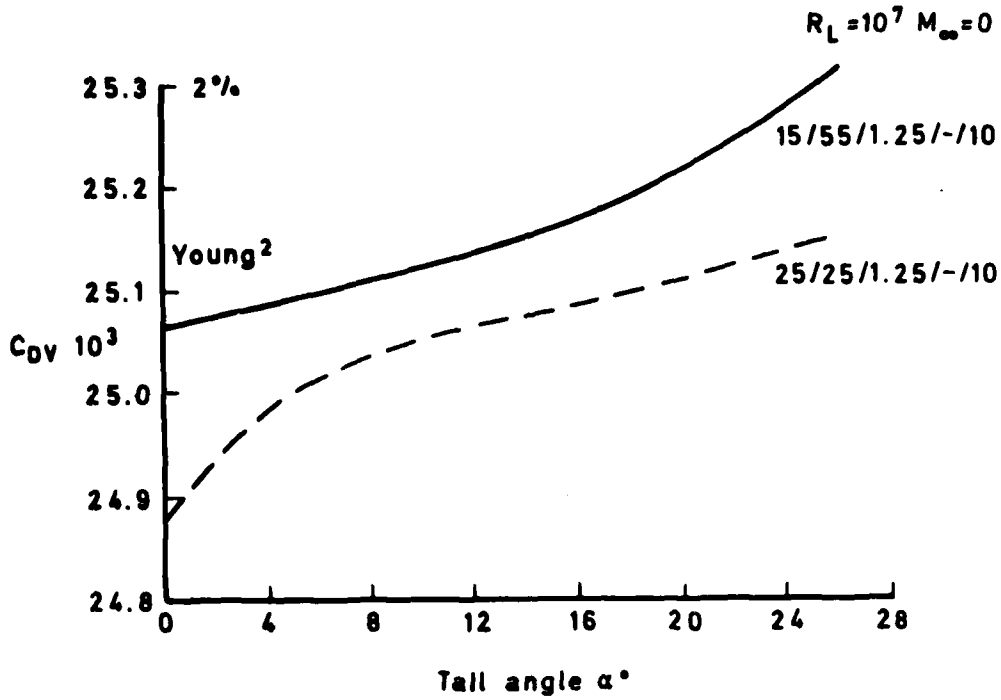

Fig 6 Effect of tail angle on drag coefficient based on volume

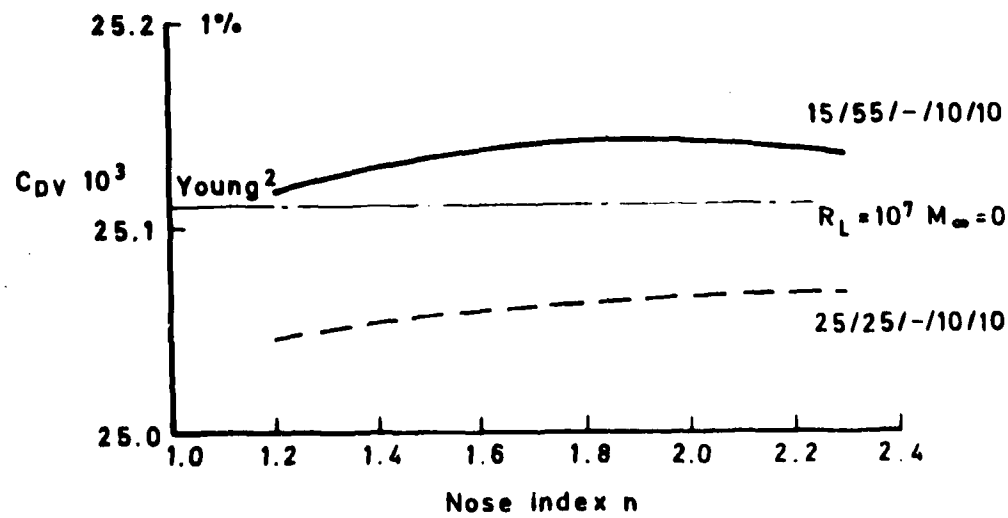

Fig 7 Effect of nose shape on drag coefficient based on volume

TR 81005

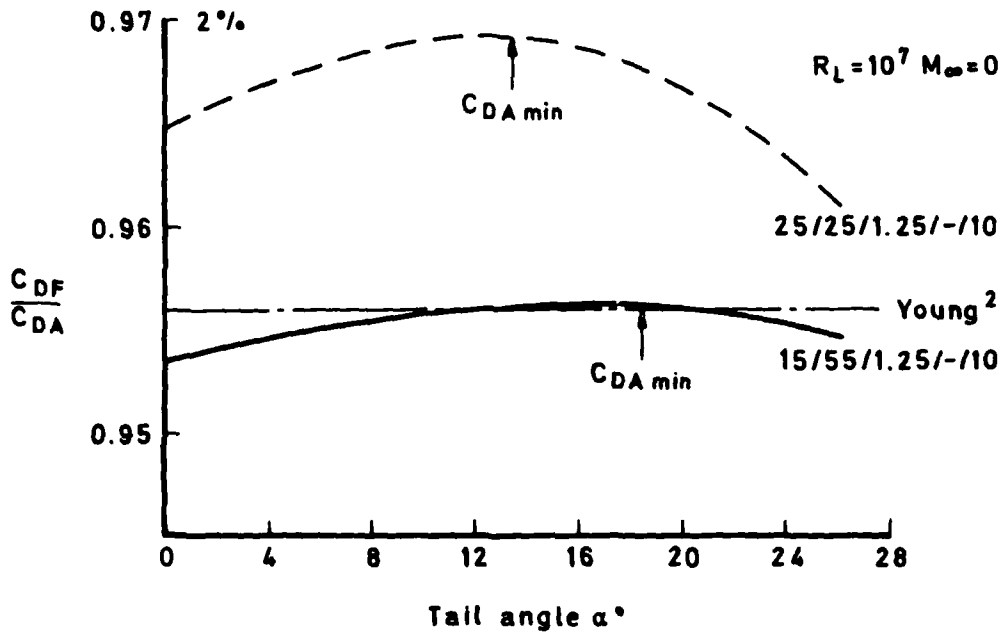

Fig 8 Effect of tail angle on the ratio of skin friction to profile drag

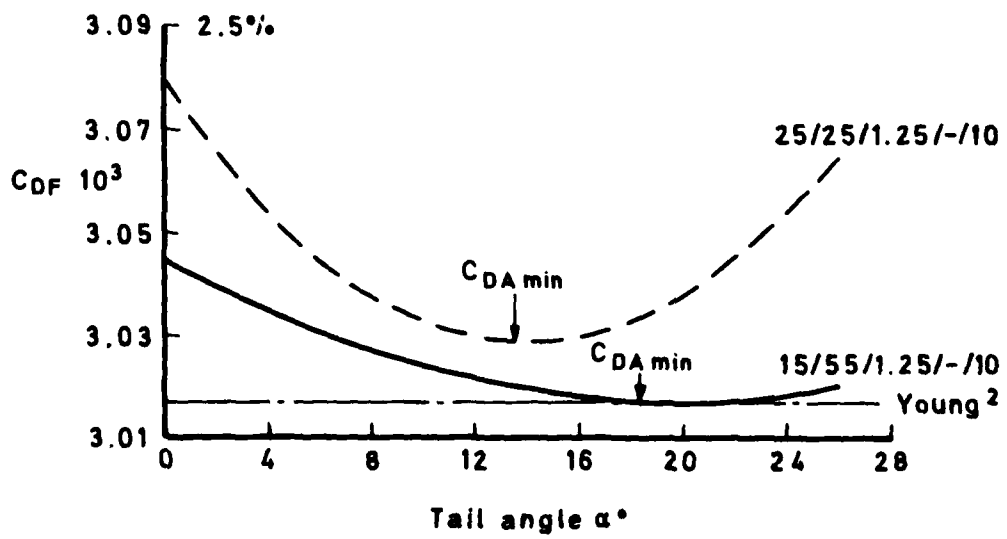

Fig 9 Effect of tail angle on skin friction drag coefficient based on surface area

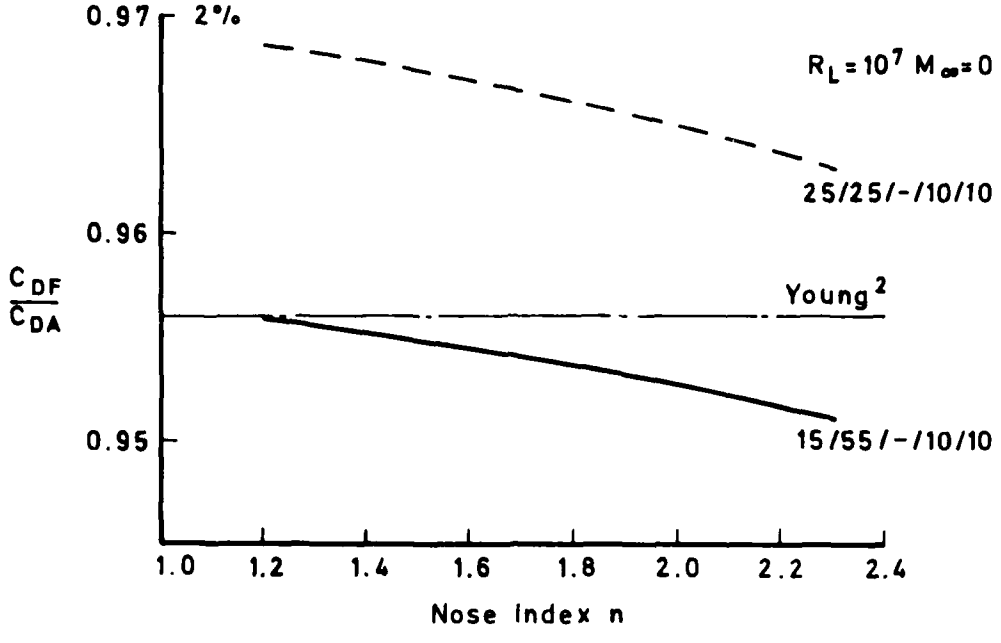

Fig 10 Effect of nose shape on the ratio of skin friction to profile drag

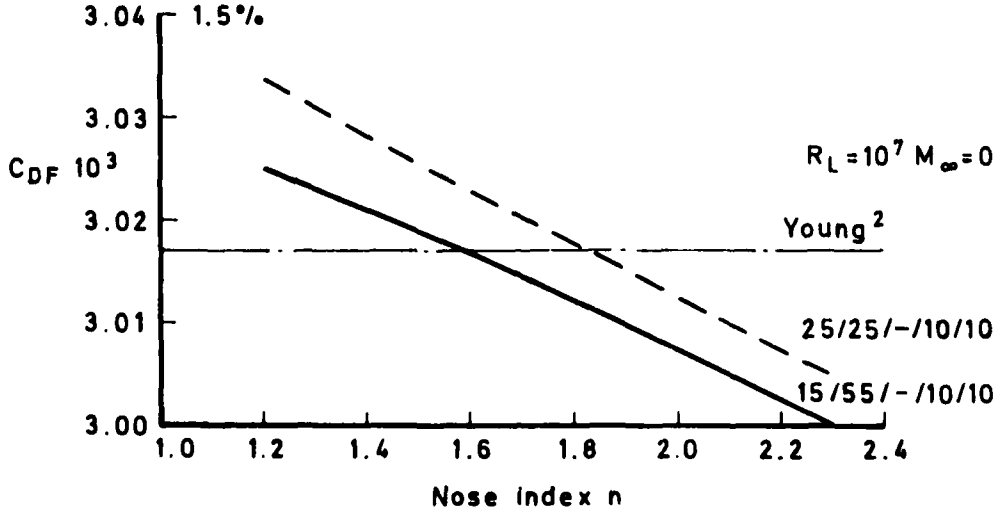

Fig 11 Effect of nose shape on skin friction drag coefficient based on surface area

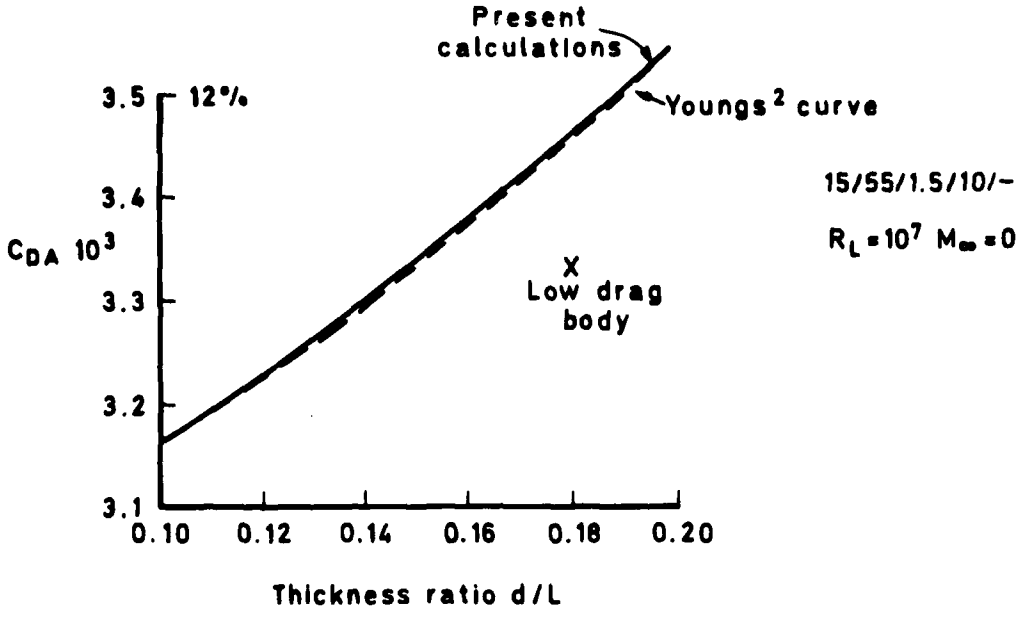

Fig 12 Effect of thickness ratio on drag coefficient based on surface area

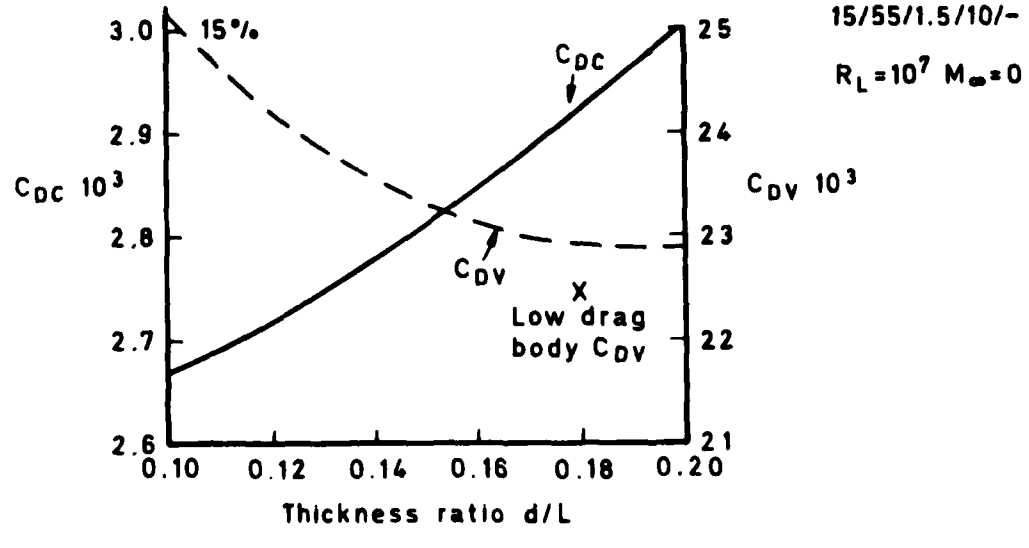

Fig 13 Effect of thickness ratio on drag coefficients based on cylinder and volume

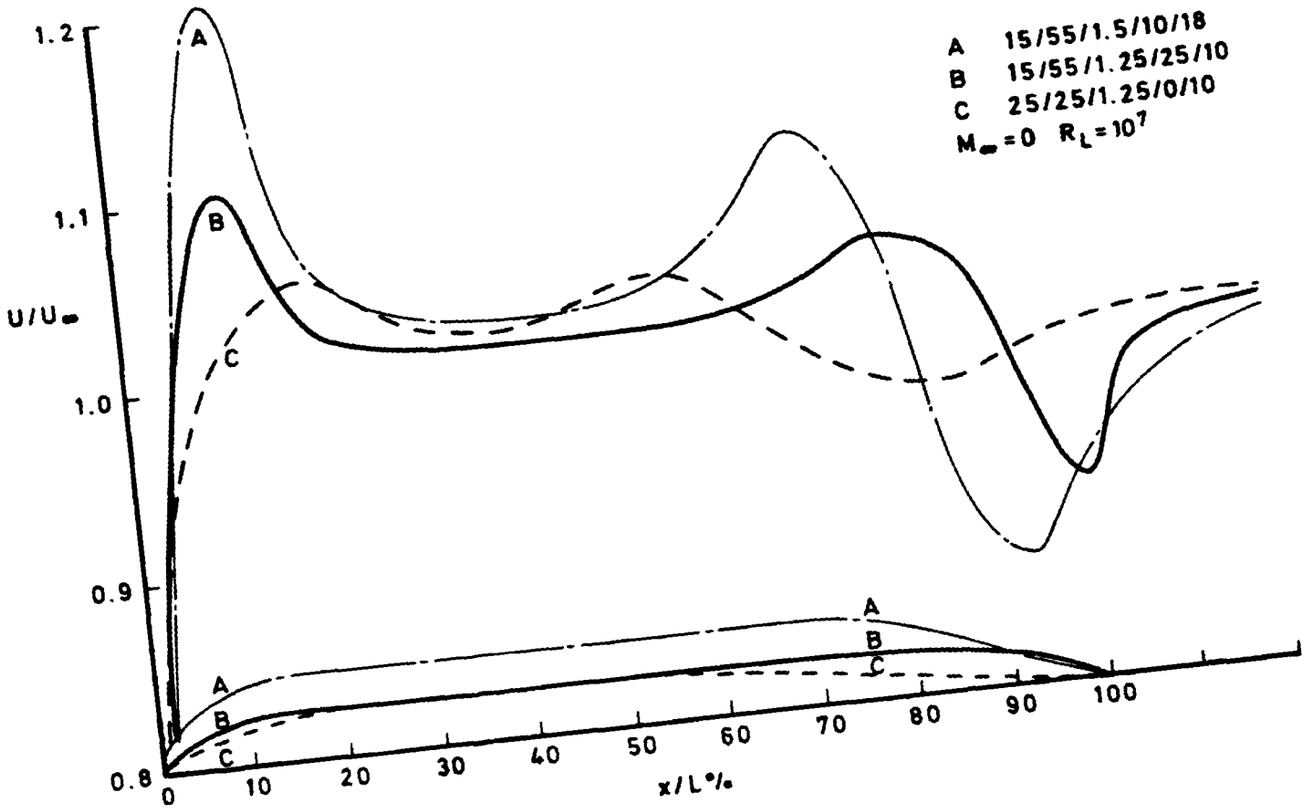

Fig 14 Effect of body shape on external flow velocity distribution

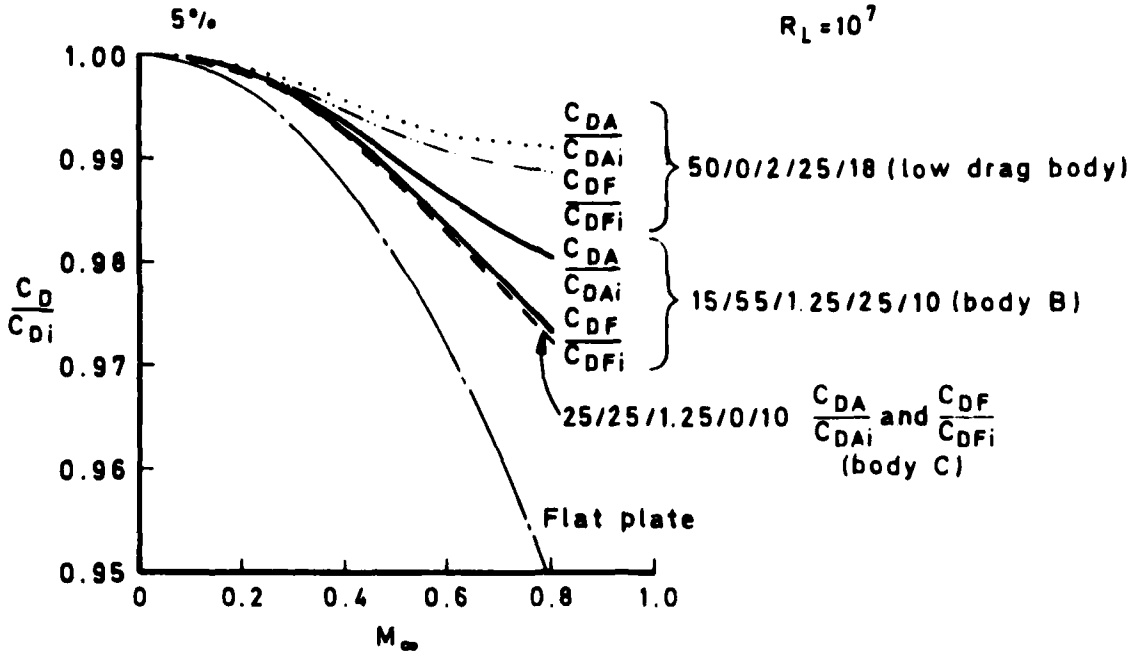

Fig 15 Effect of compressibility on profile and skin friction drags

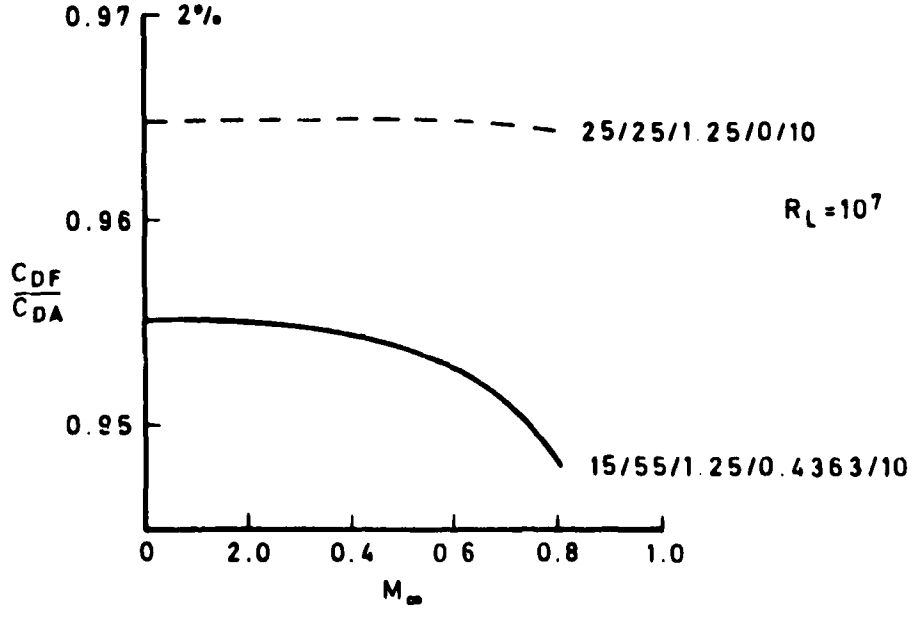

Fig 16 Effect of compressibility on the ratio of skin friction to profile drag

TR 81006

Figs 17&18

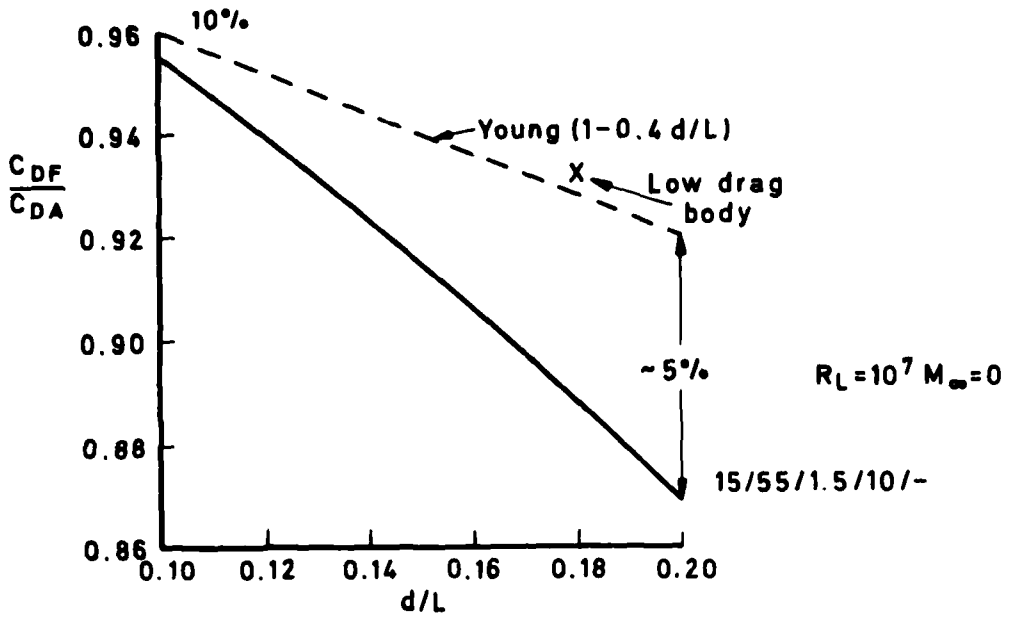

Fig 17 Effect of thickness ratio on the ratio of skin friction to profile drag

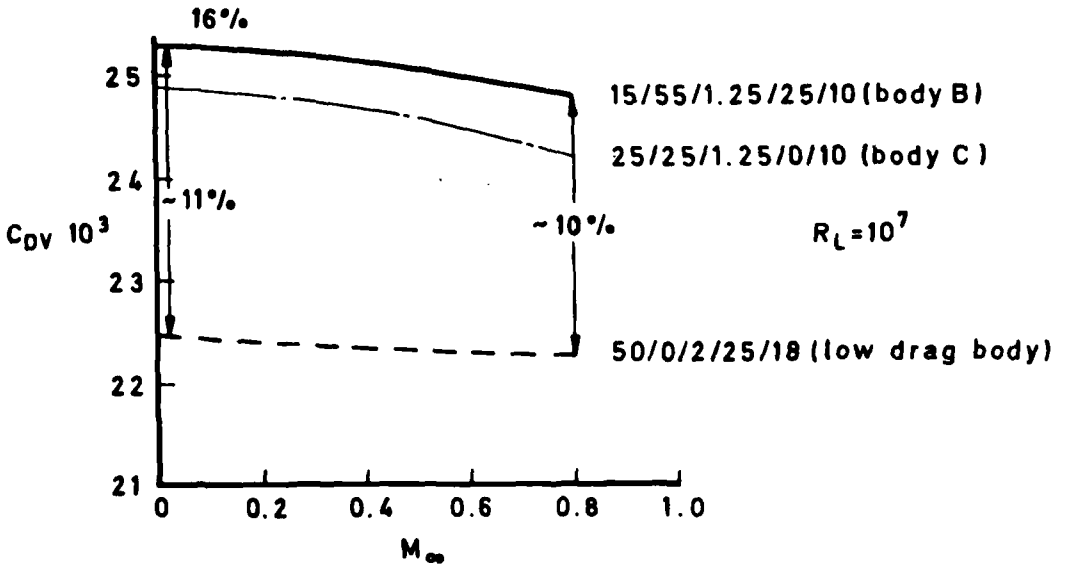

Fig 18 Effect of Mach number on drag coefficient based on volume for three bodies

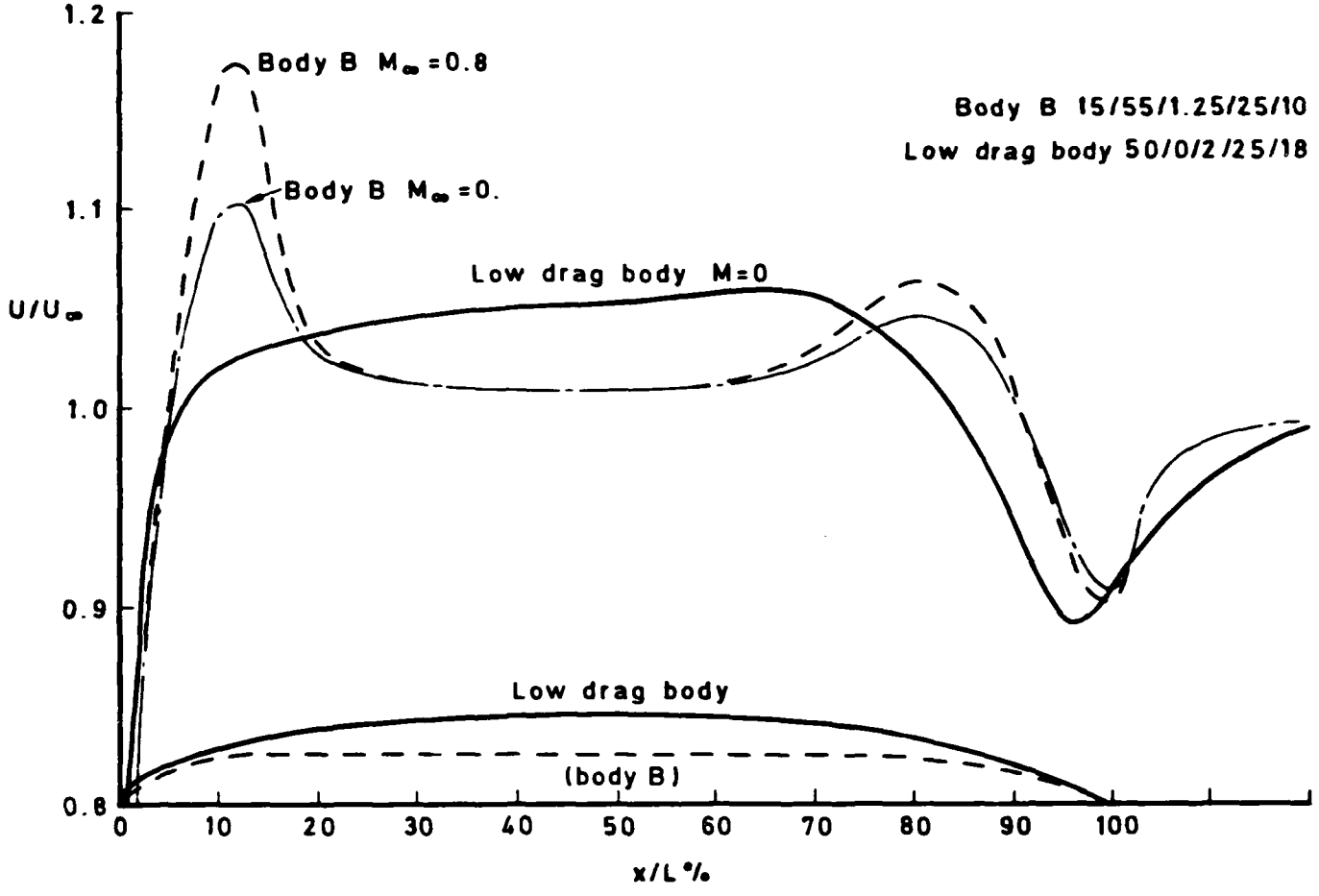

Fig 19 Comparison of velocity distributions for two bodies

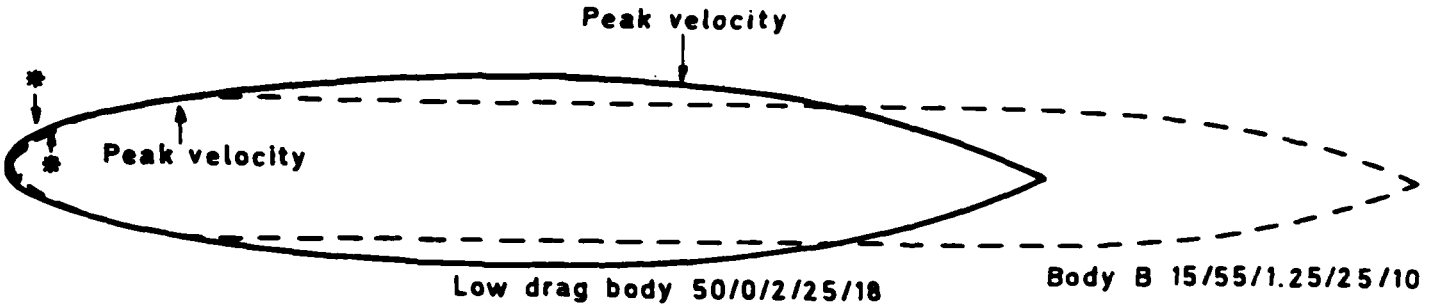

* indicates transition point

$M_\infty = 0$

	Body B	Low drag body
Peak velocity	1.101	1.057
Position of peak velocity x/L	12%	65%
R_L	$1.361.10^7$	10^7
C_{DV}	0.024101	0.022470
Ratio of drags	1.0726	1

Fig 20 Drag comparison for two bodies of equal volume

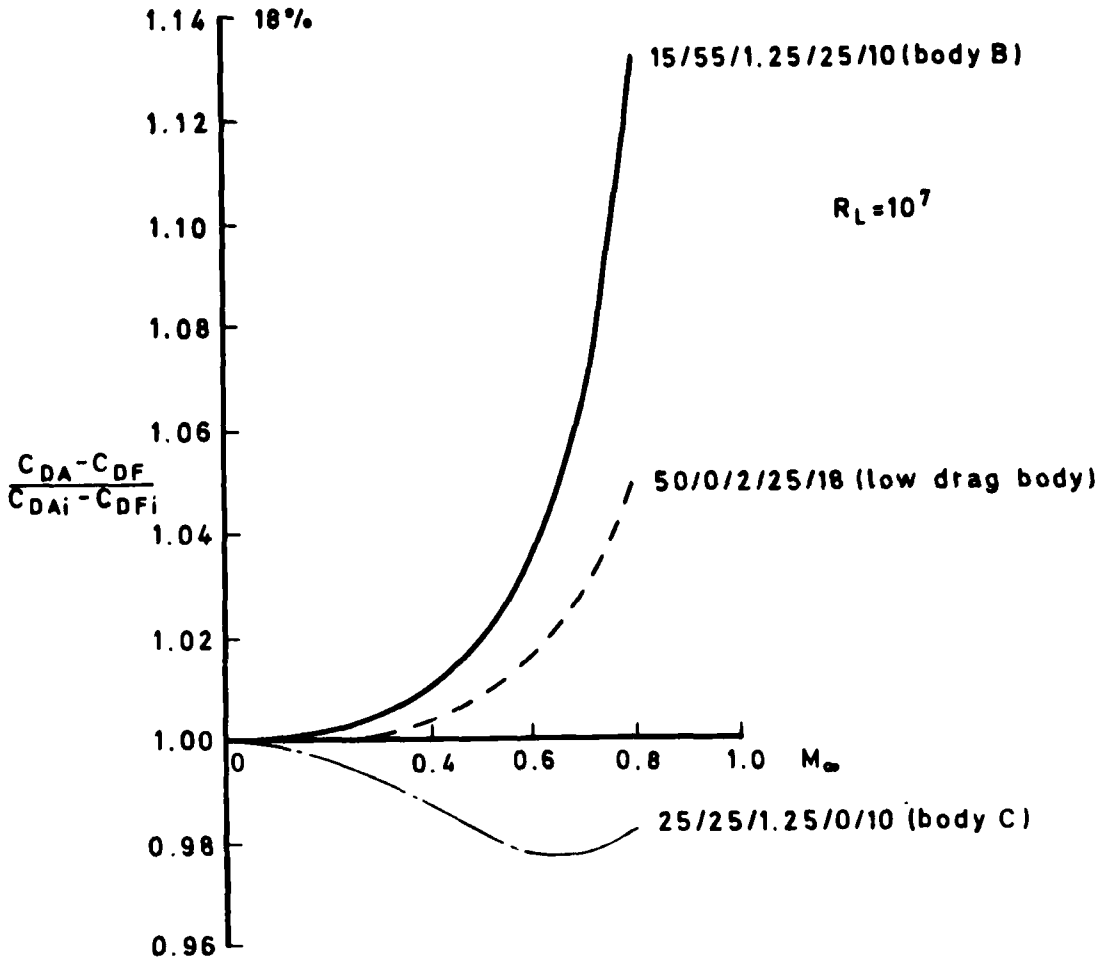

Fig 21 Effect of compressibility on form drag ($C_{DA} - C_{DF}$)

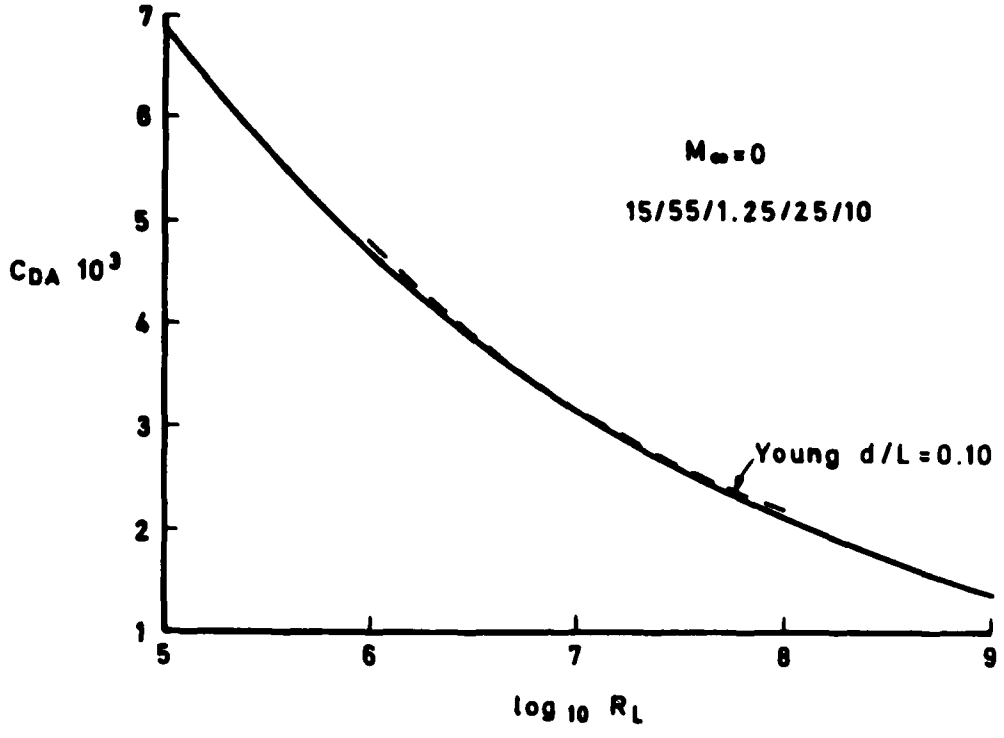

Fig 22 Effect of Reynolds number on drag coefficient based on area

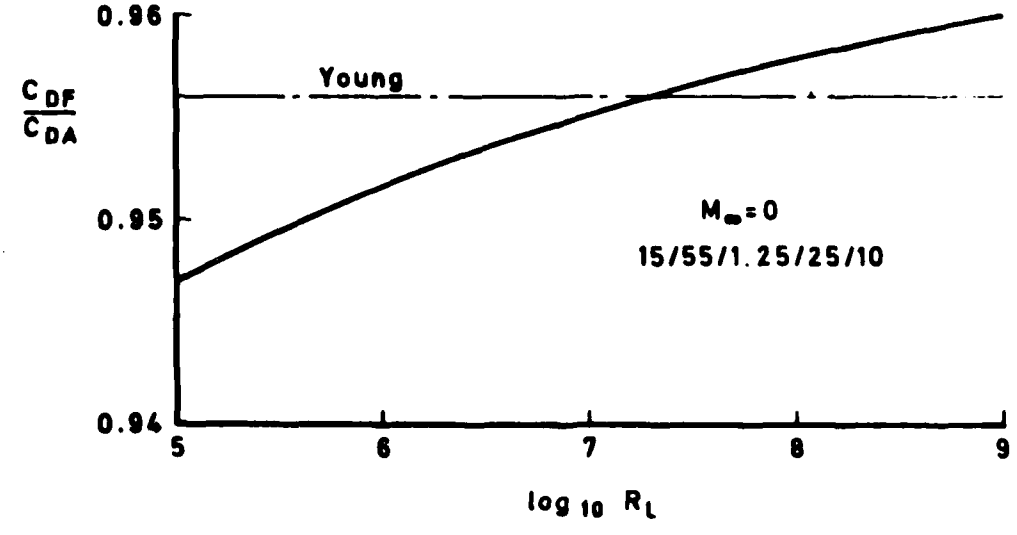

Fig 23 Effect of Reynolds number on the ratio of skin friction to profile drag

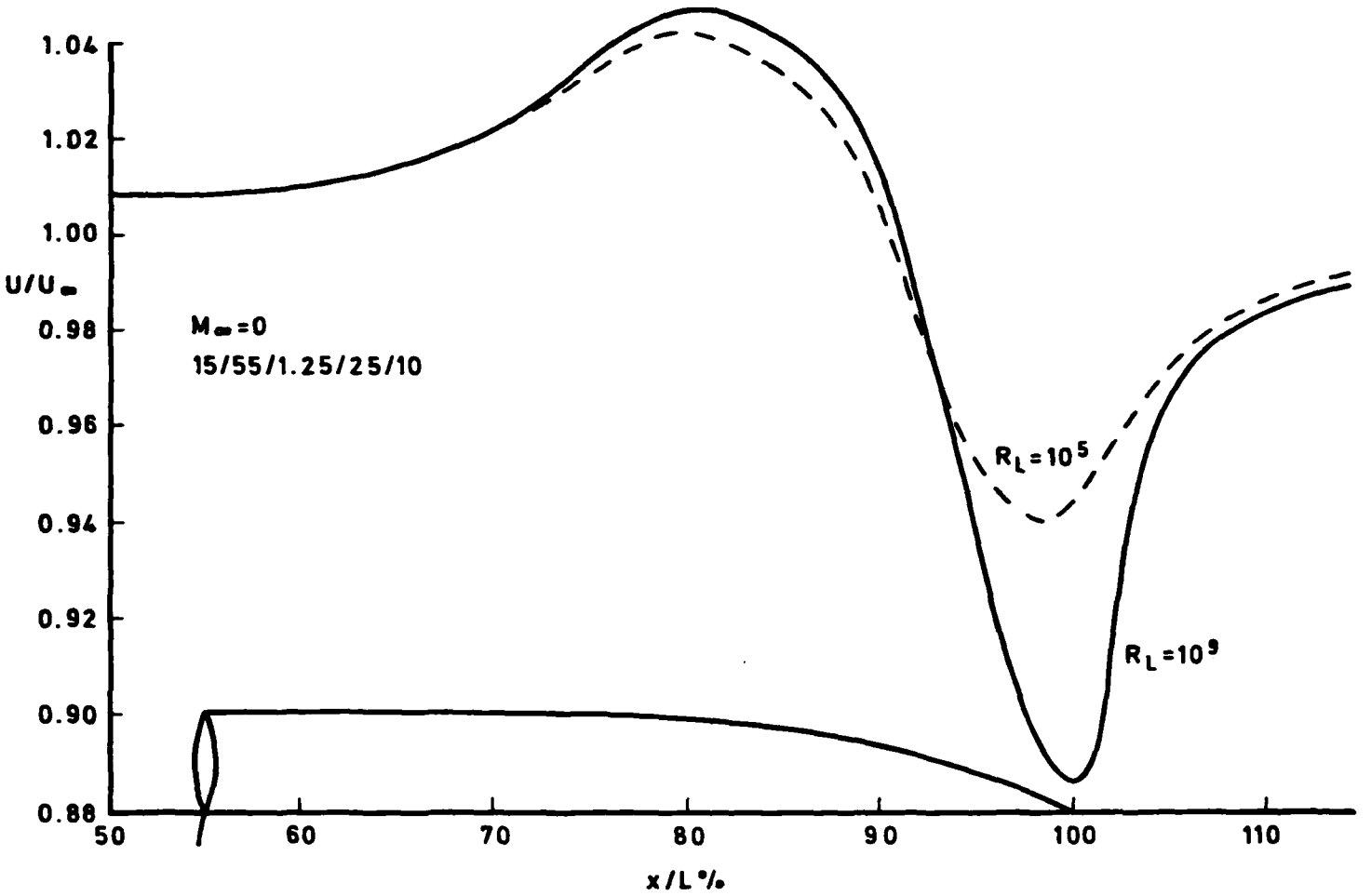

Fig 24 Effect of Reynolds number on external velocity

REPORT DOCUMENTATION PAGE

Overall security classification of this page

UNLIMITED

As far as possible this page should contain only unclassified information. If it is necessary to enter classified information, the box above must be marked to indicate the classification, e.g. Restricted, Confidential or Secret.

1. DRIC Reference (to be added by DRIC)	2. Originator's Reference	3. Agency Reference	4. Report Security Classification/Marking
	RAE TR 81005	N/A	UNLIMITED

5. DRIC Code for Originator	6. Originator (Corporate Author) Name and Location
7673000W	Royal Aircraft Establishment, Farnborough, Hants, UK
5a. Sponsoring Agency's Code	6a. Sponsoring Agency (Contract Authority) Name and Location
N/A	N/A

7. Title A theoretical study of the effects of body shape and Mach number on the drag of bodies of revolution in subcritical axisymmetric flow

7a. (For Translations) Title in Foreign Language

7b. (For Conference Papers) Title, Place and Date of Conference

8. Author 1. Surname, Initials	9a. Autnor 2	9b. Authors 3, 4	10. Date	Pages	Refs.
Myring, D.F.			January 1981	34	10

11. Contract Number	12. Period	13. Project	14. Other Reference Nos.
N/A	N/A		Aero 3496

15. Distribution statement
(a) Controlled by –
(b) Special limitations (if any) –

16. Descriptors (Keywords) (Descriptors marked * are selected from TEST)

Drag. Bodies of revolution. Shape. Axisymmetric flow.

17. Abstract

Theoretical results of profile drag calculations for bodies of revolution at zero incidence in a uniform flow are presented for a range of body shapes and Mach numbers. At a fixed fineness ratio, nose and tail contours are shown to have little influence on the profile drag coefficient based on body volume to the power 2/3. Comparison with the ESDU data sheets shows good agreement. Results of a low drag study are shown to indicate that in terms of volume enclosed a body with a fineness ratio of about 5.5 is optimum and that a continuously changing radius distribution gives rise to a slightly lower drag than that of a body having a parallel-sided central section.

F5910/1

RAE Form A143